JOURNAL OF PROPULSION AND POWER
Vol. 15, No. 4, July–August 1999

Influence of Turbulence Modeling on the Performance Prediction for Rocket Engine Nozzles

Frank A. Haidinger*
Daimler–Benz Aerospace, 81663 Munich, Germany

The flow through a nozzle of an advanced rocket engine with and without the injection of a cooling film has been studied using a Navier–Stokes method. The main focus of this study is the influence of the choice of the turbulence model on the performance prediction of a film-cooled nozzle. Results obtained demonstrate that an algebraic model significantly underestimtes the thrust and specific impulse of a nozzle. It is shown that there are remarkable differences between the predictions of the turbulence models for the loss in nozzle performance caused by the cooling of the wall.

Nomenclature

c	= sonic velocity
c_f	= skin friction coefficient
F_{I,η_i}	= inviscid fluxes
$F(Ma_t)$, F_1	= functions in the turbulence models
F_{V,η_i}	= viscous fluxes
h	= enthalpy
$I_{\text{sp, vac}}$	= specific impulse of engine at vacuum conditions
J	= metric Jacobian
k	= turbulent kinetic energy
L	= reference length
Ma	= Mach number
Ma_t	= turbulent Mach number
Pr	= Prandtl number
Pr_t	= turbulent Prandtl number
p	= pressure
p_d	= pressure dilatation
$\boldsymbol{Q}$	= conservative solution vector
q	= heat flux
Re	= Reynolds number
Re_t	= turbulent Reynolds number
t	= time
U	= velocity
u_1, u_2, u_3	= Cartesian velocity components
x_1, x_2, x_3	= Cartesian coordinates
y	= wall normal distance
$\alpha, \alpha_1, \alpha_2$	= turbulence model constants
β, β^*	= turbulence model constants
γ	= turbulence model constant
δ_{ij}	= Kronecker delta function
ε_c	= compressible dissipation
η_1, η_2, η_3	= curvilinear coordinate components
κ	= von Karman constant
μ	= molecular viscosity
μ_t	= turbulent viscosity
ρ	= density
$\sigma, \sigma^*, \sigma_2$	= turbulence model constants
υ	= shear stress
ω	= turbulent dissipation rate

Subscripts

c	= chamber value
t	= turbulent quantity
w	= wall value
∞	= freestream value

Presented as Paper 97-2808 at the AIAA/ASME/SAE/ASEE 33rd Joint Propulsion Conference, Seattle, WA, 6–9 July 1997; received 9 October 1997; revision received 20 July 1998; accepted for publication 12 September 1998.

*Research Engineer, Space Infrastructure, P.O. Box 801168. Member AIAA.

I. Introduction

THE increasing need for the transportation of payload into Earth orbit and the increasing weight of payload, sets up the challenge for the development of new launch systems and more powerful rocket engines.

The increasing chamber pressure and temperature of newly developed engines decrease the safety margins of the materials available today. Large efforts, such as the injection of cooling films, must be made to ensure that the heat transfer does not damage the structure. The limits are pushed forward into a regime where handbook methods and commonly used engineering tools reach the limits of their validity. This strengthens the need for the application of advanced development tools such as computational fluid dynamics (CFD) methods in the design process of next-generation rocket engines.

During the past years, efficient numerical schemes for the solution of the compressible Navier–Stokes equations have been developed and verified. Their main advantage is the universal applicability without calibration for each newly developed type of engine (which is usually not the case for engineering methods). It has been demonstrated successfully that these CFD methods can be used as an efficient design tool.[1]

Among the most important flow phenomena occurring in nozzle flows are the chemical reaction processes of the gases in the flow and the turbulent motion of the flow. Particularly for film-cooled nozzles, the turbulent mixing of the injected film and the main stream decides on the length, and thus, the efficiency of the cooling film. Therefore, some recent studies of film cooling for advanced nozzle design concentrated on the basic flow phenomena, such as wall heat transfer, turbulent mixing of the film, and the main jet and cooling film stability.[2–4]

While the development of turbulence models for incompressible flows has reached a state where flows can be predicted for engineering purposes with at least reasonable accuracy, the database of compressible flow experiments for the development of turbulence models is small. Therefore, it is necessary to verify turbulence models used for the calculation of high-speed flows by a careful comparison to reliable experiments, and to assess the uncertainty in the flow prediction for relevant nozzle-design criteria. Under this light, the present study has been conducted to get an impression of the impact of turbulence modeling on the performance prediction for film-cooled nozzles.

II. Numerical Method

An accurate and efficient way to predict the performance of a nozzle is the solution of the Favre-averaged Navier–Stokes equations for selected points of the operating envelope of the engine.

Basic equations for the viscous flow of an equilibrium real gas in a generalized coordinate system (η_1, η_2, η_3) can be written in the form

$$\frac{\partial \boldsymbol{Q}}{\partial t} J^{-1} + \sum_{i=1}^{3} \frac{\partial}{\partial \eta_i}\left(F_{I,\eta_i} - Re_\infty^{-1} F_{V,\eta_i}\right) = 0 \tag{1}$$

with $\boldsymbol{Q} = (\rho, \rho u_1, \rho u_2, \rho u_3, e)^T$; the inviscid fluxes F_{I,η_i}; and the viscous fluxes F_{V,η_i}. J is given by $J = \partial(\eta_1, \eta_2, \eta_3)/\partial(x_1, x_2, x_3)$; the Reynolds number is defined by the reference values $Re = \rho_\infty U_\infty L/\mu_\infty$.

The Favre-averaged Navier–Stokes equations [Eq. (1)] are solved by an implicit second-order finite volume Newton-type relaxation scheme. The derivatives of the inviscid fluxes are approximated by a symmetric total variation diminishing scheme,[5,6] using a Roe-averaged four-argument minmod limiter.[7,8] Second-order derivatives are expressed by central differences. At each time step, a Newton method with a line Gauss–Seidel relaxation in alternating directions is employed to compute the solution. The equilibrium real gas properties are calculated using spline functions from surfaces of state (generated using the NASA Lewis Research Institute code[9]).

Thrust and specific impulse of the nozzle are evaluated by the integration of pressure, density, and velocity (impulse), over the exit plane of the nozzle. To check for the convergence of the calculation, the mass flux is evaluated at several cross sections of the nozzle.

A more detailed presentation of the numerical method, together with a description of the implementation of the two-equation turbulence models, can be found in Refs. 10 and 11.

III. Turbulence Modeling

A. Algebraic Models

A common approach for industrial applications is the use of algebraic eddy–viscosity turbulence models for the description of the turbulent behavior of the flow. Their main advantages are a simple implementation in the numerical method and an acceptable accuracy of the solution for a variety of flow problems.

In the present study, the popular Baldwin–Lomax model (BLM)[12] has been used as a basic reference. It is based on Prandtl's mixing-length hypothesis, and requires damping terms to mimic near-wall behavior and far-wall intermittency.

A more recent approach in algebraic turbulence modeling is based on the renormalization group (RNG) theory introduced by Yakhot and Orszag.[13] While an RNG model is functionally the same as a mixing length model, it does not require damping functions or empirical boundary-layer transition models. This makes it a viable alternative to the traditional mixing-length models for complex three-dimensional flows. Under this light, the model of Kirtley[14] has been chosen to study the potential of algebraic RNG models for the prediction of complex nozzle flows.

B. Two-Equation Models

A more sophisticated ansatz to model the turbulence in the flow is the solution of additional equations for a turbulent velocity scale and a turbulent length scale. Within the frame of this study, k is taken as a squared velocity scale and the mean frequency of the energy containing eddies ω to determine the turbulent length scale. The equations solved additionally to the mean flow equations are given in a general form by

$$\frac{\partial \rho k}{\partial t} + \frac{\partial \rho k u_j}{\partial x_j} - \left(1 - \alpha_1 Ma_t^2\right)\upsilon_{ij}\frac{\partial u_i}{\partial x_j} + \left[1 + \alpha F(Ma_t) - \alpha_2 Ma_t^2\right]\beta^* \rho \omega k - \frac{\partial}{\partial x_j}\left[\left(\mu + \sigma^* \mu_t\right)\frac{\partial k}{\partial x_j}\right] = 0 \tag{2}$$

$$\frac{\partial \rho \omega}{\partial t} + \frac{\partial \rho \omega u_j}{\partial x_j} - \left(\gamma + \alpha_1 Ma_t^2\right)\frac{\rho}{\mu_t}\upsilon_{ij}\frac{\partial \mu_i}{\partial x_j} + \left[\frac{\beta}{\beta^*} - \alpha F(Ma_t) + \alpha_2 Ma_t^2\right]\beta^* \rho \omega^2 - \frac{\partial}{\partial x_j}\left[(\mu + \sigma \mu_t)\frac{\partial \omega}{\partial x_j}\right] - (1 - F_1)\sigma_2 \frac{2\rho}{\omega}\frac{\partial k}{\partial x_j}\frac{\partial \omega}{\partial x_j} = 0 \tag{3}$$

with

$$\upsilon_{ij} = \mu_t\left(\frac{\partial u_i}{\partial x_j} + \frac{\partial u_j}{\partial x_i} - \frac{2}{3}\delta_{ij}\frac{\partial u_k}{\partial x_k}\right) - \frac{2}{3}\delta_{ij}\rho k \tag{4}$$

Five models were selected for the comparison, namely, the high Reynolds number k-ω model,[15] the Wilcox hypersonic (HYP) k-ω model,[16] the low Reynolds number k-ω model,[17] the Menter baseline (BSL) model, and the Menter shear-stress transport (SST) model.[18] All models are based on the high Reynolds number version of the k-ω model.

The k-ω model is the model of choice for wall-bounded flows with complex geometries. Unlike most of the other two-equation models, the k-ω model does not need any damping functions in the wall vicinity, a feature that makes it independent from geometrical restrictions.

The two models of Menter[18] differ from the other three Wilcox models[15–17] by the reintroduction of a cross-diffusion term, which has been neglected by Wilcox in his approach. Formally, this transforms the k-ω model into a k-ε model. Because the cross-diffusion term is damped by a blending function in the vicinity of a wall, the Menter models show a very similar behavior near walls as the k-ω models, but avoid the known sensitivity to freestream values of the k-ω model. An additional advantage of the Menter SST model is an improved performance for adverse pressure gradient flows because of a modification of the eddy viscosity to account for the anisotropic behavior of the turbulent shear stress. Table 1 summarizes all models used in this study.

The basic models, presented earlier (except for the HYP model[16]), are models for incompressible turbulence. They can be applied to compressible flows within the validity range of Morkovin's hypothesis, that fluctuations of total temperature and pressure are much smaller than their mean values. For boundary-layer flows, this is the case up to Mach numbers at the boundary-layer edge of about 4–5.

Several studies of compressibility effects in turbulence have indicated that dilatational effects, namely, compressible dissipation ε_c and pressure dilatation p_d, may play a role for hypersonic flows.[19,20] Therefore, the model of Zeman,[21] for the compressible dissipation, and the model of Sarkar et al.,[22] for the pressure dilatation, have been included:

$$\alpha = 0.75, \qquad F(Ma_t) = 1 - \exp\left[-(Ma_t - 0.25)^2/0.66^2\right]$$
$$\alpha_1 = 0.4, \qquad \alpha_2 = 0.2, \qquad Ma_t = \sqrt{2k}/c \tag{5}$$

In the case of the HYP model, the original model constants have been used:

$$\alpha = 1.5, \qquad F(Ma_t) = Ma_t^2 - 0.25^2$$
$$\alpha_1 = 0, \qquad \alpha_2 = 0 \tag{6}$$

The turbulent heat flux in the energy equation is assumed to be proportional to the mean temperature gradient, so that

$$q_{T_j} = -\frac{\mu_t}{Pr_t}\frac{\partial h}{\partial x_j} \tag{7}$$

where the turbulent Prandtl number is assumed to be 0.90.

IV. Results

A. Validation of Prediction Accuracy

For the validation of the code, the performance of the nozzle of an existing engine has been calculated using various turbulence

Table 1 Constants and damping functions for the turbulence models

Turbulence model	β	β^*	γ	σ	σ^*	κ	μ_t	σ_2	F_1
WHR[15]	0.075	0.09	$\frac{5}{9}$	0.5	0.5	0.41	$\rho k/\omega$	0	1
HYP[16]	0.075	0.09	$\beta/\beta^* - \sigma\kappa^2/\sqrt{\beta^*}$	0.5	0.5	0.41	$\rho k/\omega$	0	1
WLR[17]	0.075	$0.09\frac{\frac{5}{18}+(Re_t/8)^4}{1+(Re_t/8)^4}$	$\frac{5}{9}\frac{0.1+Re_t/2.7}{1+Re_t/2.7}\frac{1+Re_t/6}{\beta/3+Re_t/6}$	0.5	0.5	0.41	$\frac{\beta/3+Re_t/6}{1+Re_t/6}\frac{\rho k}{\omega}$	0	1
BSL[18]	$0.075F_1+0.0828(1-F_1)$	0.09	$\beta/\beta^* - \sigma\kappa^2/\sqrt{\beta^*}$	$0.5F_1+\sigma_2(1-F_1)$	$0.5F_1+(1-F_1)$	0.41	$\rho k/\omega$	0.856	$\tanh(\arg_1^4)$
SST[18]	$0.075F_1+0.0828(1-F_1)$	0.09	$\beta/\beta^* - \sigma\kappa^2/\sqrt{\beta^*}$	$0.5F_1+\sigma_2(1-F_1)$	$0.85F_1+(1-F_1)$	0.41	$\frac{0.31\rho k}{\max[0.31\omega, \|\Omega\|\tanh(\arg_2^2)]}$	0.856	$\tanh(\arg_1^4)$

Note: $\arg_1 = \min\left[\max\left(\frac{\sqrt{k}}{0.09\omega y}, \frac{500\mu}{\rho\omega y^2}\right), \frac{4\rho k\sigma_2}{CD_{k\omega}y^2}\right]$; $CD_{k\omega} = \max\left(\frac{2\rho\sigma_2}{\omega}\frac{\partial k}{\partial x_j}\frac{\partial\omega}{\partial x_j}10^{-20}\right)$; $\arg_2 = \max\left(\frac{2\sqrt{k}}{0.09\omega y}, \frac{500\mu}{\rho\omega y^2}\right)$; $Re_t = \frac{\rho k}{\mu\omega}$.

Table 2 Validation of turbulence models

Turbulence model	Level	$\Delta I_{sp,vac}$
BLM	Algebraic model	−3.2 s
WHR	Two-equation model	+0.2 s
HYP	Two-equation model	+0.1 s
BSL	Two-equation model	+0.1 s
SST	Two-equation model	+0.0 s
WLR	Two-equation model	+2.8 s
WHR + $\varepsilon_c + p_d$	Two-equation model	+3.4 s

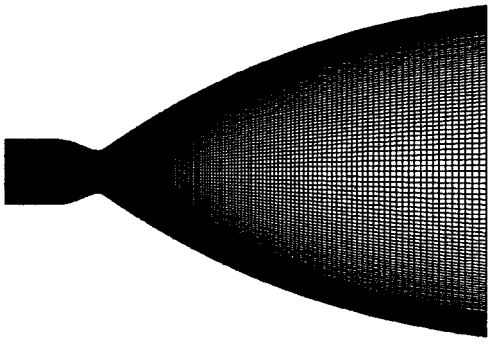

Fig. 1 Computational grid, validation case.

models. The nozzle geometry and the computational grid (80 × 256 cells, axisymmetric) are shown in Fig. 1. The boundary layer has been resolved with about 30–40 cells, with the cell center of the first cells at a wall lower than $y^+ = 0.5$.

The flow conditions used were given by the chamber pressure $P_c \approx 101$ bar, and the mixing ratio (O/F) of H_2 and $O_2 \approx 5.9$, as an average from a series of several thrust chamber tests of the engine. Because the nozzle is actively cooled by a dump flow in cooling channels down until the nozzle exit, the wall temperature distribution was prescribed as a linear distribution between experimental data. At the nozzle exit, all flow variables have been extrapolated to the exterior, and at the axis, a symmetry condition has been applied.

Calculations have been made for turbulent flow using the algebraic BLM and a variety of two-equation models of the k-ω type. The primary results of the calculations are thrust, effective specific impulse, and wall pressure distribution for the given contour.

As a result, from the evaluation of the test data, a measured specific impulse can be given. In the thrust chamber tests, several effects are present, which influence the performance, but are not simulated by the numerical investigation. Among the most important of these effects are the incomplete combustion in the chamber, the deformation of the nozzle by thermal and mechanical loads, the impurity of the propellants, the base pressure, and the thrust from the dump flow, which is expanded by small nozzles at the end of the cooling channels. Thus, the measured specific impulse is not directly comparable with the numerical value.

Because the thrust chamber efficiency (loss caused by incomplete combustion) is dominating all of the other effects, it is possible to make an estimate for these minor effects. The missing effect from the incomplete combustion is determined by tests with a subscale version of the chamber. Thus, a final reference value for the specific impulse from the experiment can be given. For the comparison of the numerical performance predictions, the deviation from the experimental reference value for the specific impulse under vacuum conditions $\Delta I_{sp,vac}$ is evaluated (Table 2).

The comparison between numerical and experimental data shows that the algebraic BLM gives a sufficiently lower value for the specific impulse, whereas most of the two-equation models predict values close to the experimental reference value. Only the low-Re version of the k-ω model and the standard k-ω model with compressibility effects included predict values higher than the experimental reference value.

The wall pressure distribution (Fig. 2) shows a good agreement of all two-equation models, whereas the BLM differs from all other models. The skin friction (Fig. 3) predicted by the BLM is sufficiently larger than the prediction of the two-equation models. This increased wall friction induces the underprediction of the specific impulse. The decreased friction in the case of the Wilcox low Re (WLR) and the extended Wilcox high Re (WHR) (with dilatational effects included) leads to an overprediction of the specific impulse by these two models.

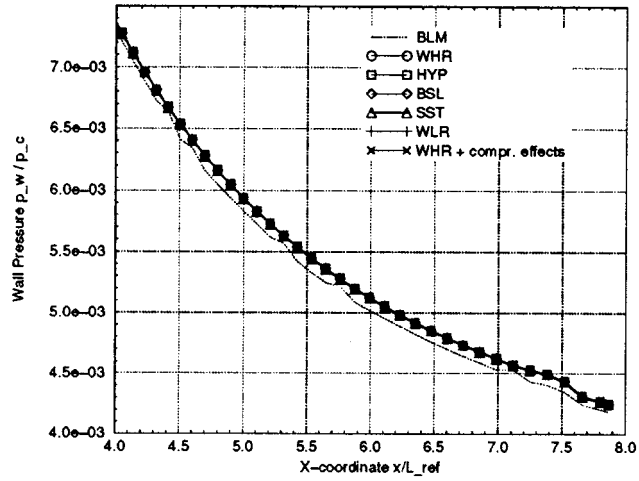

Fig. 2 Wall pressure distribution, validation case.

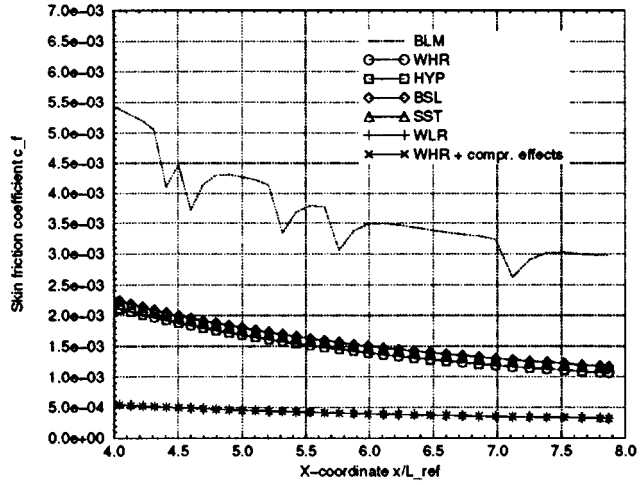

Fig. 3 Skin friction distribution, validation case.

It is interesting to see that the HYP model, which has an ansatz for the compressible dissipation included, does not overpredict the specific impulse in contrast to the extended WHR. This indicates that the strong decrease in skin friction observed with this model is a result of the influence of the pressure dilatation terms. This is not surprising because there are some indications for some deficiencies in the modelization of compressibility effects in turbulence.

Finally, it should be mentioned that the waviness in the wall pressure and the skin friction in the case of the BLM is caused by the variation in the prescribed wall temperature. This variation has no visible influence on the skin friction predicted by the two-equation models.

B. Performance Prediction for Clean Nozzle Flow

During the design process of a nozzle, it is important to study all effects influencing the performance of the nozzle. For a better understanding of the effects, we first study them on a clean nozzle operated at the same chamber conditions as the film-cooled nozzle. These were given by the chamber pressure $P_c = 117$ bar and the mixing ratio (O/F) of H_2 and $O_2 = 7.2$.

The contour of a generic film-cooled nozzle has been designed as a basic contour with two steps of constant height for the two-staged injection of the cooling film. This basic contour is taken as the

Table 3 Influence of the wall temperature, clean nozzle[a]

Turbulence model	Level	$\Delta I_{sp,vac}$
BLM	Algebraic model	−5.6 s
SST	Two-equation model	−2.6 s

[a]Difference between adiabatic and cold wall.

Table 4 Influence of turbulence modeling, clean nozzle

Turbulence model	Level	$\Delta I_{sp,vac}$	Wall
SST	Two-equation model	Reference	Adiabatic
BLM	Algebraic model	−3.2 s	Adiabatic
SST	Two-equation model	Reference	Cold
BLM	Algebraic model	−6.2 s	Cold
RNG	Algebraic model	−5.4 s	Cold
WHR	Two-equation model	+0.2 s	Cold
HYP	Two-equation model	+0.0 s	Cold
BSL	Two-equation model	+0.0 s	Cold

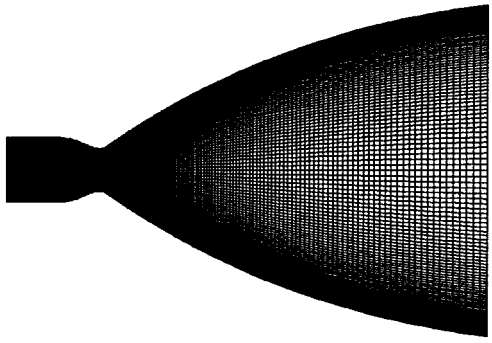

Fig. 4 Computational grid, clean nozzle.

contour of the clean nozzle. The contour and the computational grid (20,480 cells, axisymmetric) used for the computations is shown in Fig. 4. The boundary layer has been resolved with about 30–40 cells, with the cell center of the first cells at a wall lower than $y^+ = 0.5$. Again, at the nozzle exit, all flow variables have been extrapolated to the exterior, and at the axis, a symmetry condition has been applied. At the wall, a no-slip condition has been implemented.

Based on the results presented in the preceding text, the SST model is chosen as a reference model for the performance prediction.

In the case of the generic nozzle contour used for this study, as well as during early stages of the design process of a nozzle, the cooling channels, and thus, the heat transfer to the wall and the wall temperature are not defined. Therefore, a wall temperature distribution is estimated. To check the uncertainty of such an estimate, the performance is calculated for cold wall conditions and adiabatic wall conditions as well. The loss in the specific impulse, because of the cold wall $\Delta I_{sp,vac}$, is shown in Table 3 for the algebraic BLM and the Menter SST two-equation model as typical representatives of each level of turbulence modeling.

The results show a remarkable difference in the prediction of $\Delta I_{sp,vac}$ between both turbulence models. Because this cannot be explained without quantifying the influence of turbulence modeling, the impact of the choice of the turbulence model on the performance prediction for this flow is shown in Table 4.

As observed in the validation test case, two distinct levels for the specific impulse can be identified. One low level is predicted by the algebraic models, and a significantly higher one by the two-equation models. The predictions of the two-equation models are in remarkably good agreement.

Table 4 shows additionally that the difference between the predictions of the two classes of turbulence models is larger in the case of the cold wall than that for an adiabatic wall condition. This is in agreement with results from a study of the basic behavior of turbulence models presented in Ref. 19.

Mach number and pressure distribution of the calculations with the SST model (reference calculations) are shown in Figs. 5 and 6

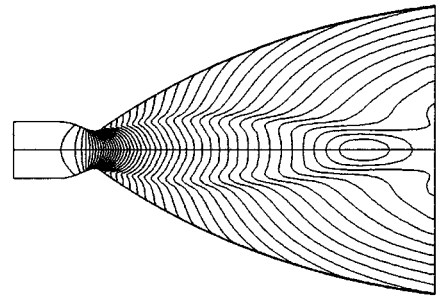

Fig. 5 Mach number distribution, adiabatic wall, clean nozzle.

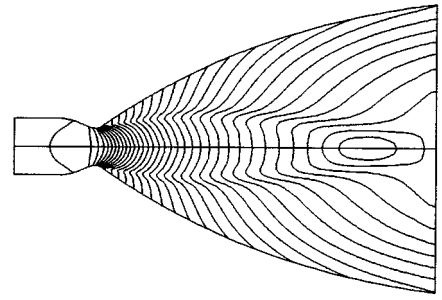

Fig. 6 Pressure distribution (log p/p_∞), adiabatic wall, clean nozzle.

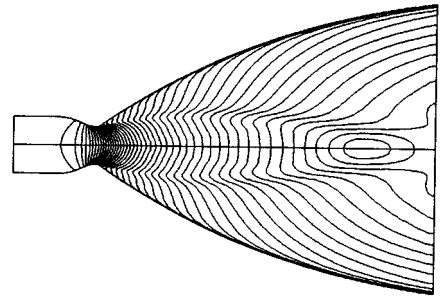

Fig. 7 Mach number distribution, cold wall, clean nozzle.

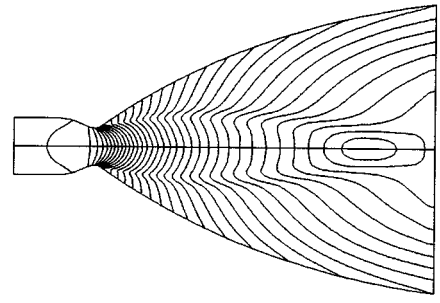

Fig. 8 Pressure distribution (log p/p_∞), cold wall, clean nozzle.

for adiabatic wall conditions, and in Figs. 7 and 8 for cold wall conditions. While there seems to be no influence on the pressure distribution, in the case of the cold wall condition an increased boundary-layer thickness can be noticed. This induces a loss in specific impulse because of increased friction losses.

C. Performance Prediction for a Nozzle with Film Injection

For the study of the influence of turbulence modeling on the performance prediction of a film-cooled nozzle, two constant steps on the clean contour are defined to simulate the two-stage injection of a cooling film.

To achieve comparable results with those of the clean nozzle, the same chamber conditions for the main flow have been used. The injection conditions for the two injected films have been chosen with

Table 5 Influence of turbulence modeling, film-cooled nozzle

Turbulence model	Level	$\Delta I_{sp,vac}$	Wall
SST	Two-equation model	Reference	Adiabatic
BLM	Algebraic model	−1.9 s	Adiabatic
SST	Two-equation model	Reference	Cold
BLM	Algebraic model	−4.0 s	Cold

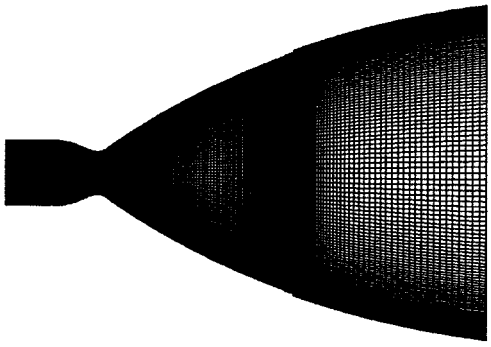

Fig. 9 Computational grid, film-cooled nozzle.

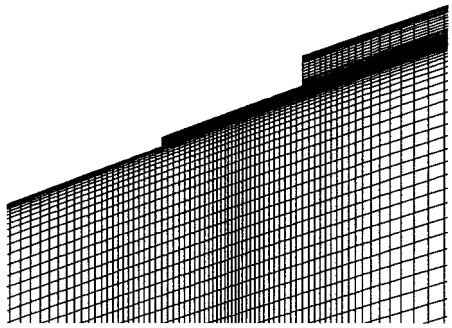

Fig. 10 Detail of computational grid, film-cooled nozzle.

static pressure matched to the wall pressure at the injection point and generic values for mass flow, total pressure, and total temperature.

The contour and the computational grid with three blocks ($80 \times 212, 112 \times 30, 148 \times 58 = 28{,}904$ cells, axisymmetric), used for the computations presented in the following, are shown in Figs. 9 and 10. The boundary layer has been resolved with about 30–40 cells, the mixing layers with more than 60 in the second block and more than 100 cells in the last block. Throughout the whole computational domain, the cell center of the first cells are closer to the wall than $y^+ = 0.5$. As in the previous cases, at the nozzle exit all flow variables have been extrapolated to the exterior, and at the axis a symmetry condition has been applied. At the wall, a no-slip condition has been implemented. Again, the Menter SST model has been chosen as the reference model for the performance prediction.

A comparison of the specific impulse predicted by the algebraic BLM to the prediction of the Menter SST two-equation turbulence model (Table 5) shows that the value of the algebraic model is significantly lower than the specific impulse predicted by the two-equation model. This is in accordance with the results obtained for the clean nozzle flow.

In comparison with the clean nozzle flow in the case of the flow with film injection, the wall boundary condition is changed downstream of the film injection. Therefore, the impact of the wall boundary condition in combination with the choice of turbulence model must be evaluated again.

As in the clean nozzle case, the specific impulse is decreased by the transfer of energy to the cooled wall (Table 6). The absolute figures of the loss in specific impulse cannot be compared with each other because of the increased mass flow in the case with film injection.

Table 6 Influence of the wall temperature, film-cooled nozzle[a]

Turbulence model	Level	$\Delta I_{sp,vac}$
BLM	Algebraic model	−4.8 s
SST	Two-equation model	−2.7 s

[a]Difference between adiabatic and cold wall.

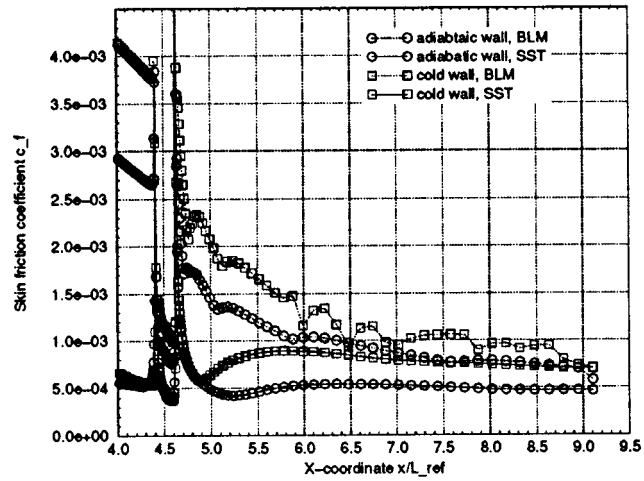

Fig. 11 Skin friction distribution, film-cooled nozzle.

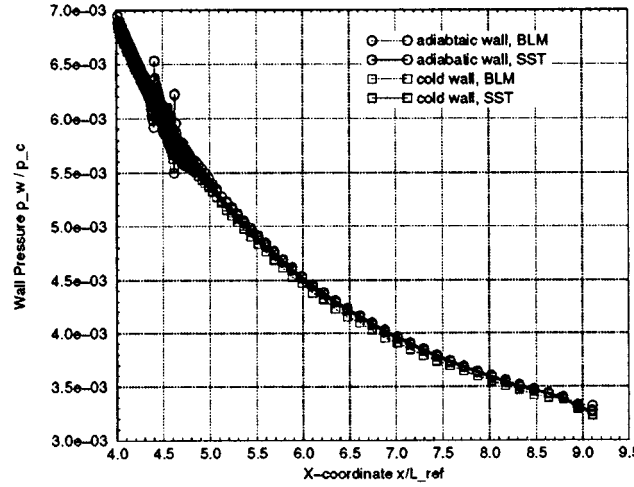

Fig. 12 Wall pressure distribution, film-cooled nozzle.

The loss in specific impulse can also be identified by the increased skin friction parameter (Fig. 11) for both turbulence models. Again, the variation in the skin friction predicted by the algebraic BLM in the cold wall case is caused by the variation in the prescribed wall temperature. The difference between the curves indicates the difference in the prediction of the specific impulse because of the changed friction loss.

Figure 12 shows that the algebraic BLM and the Menter SST two-equation model almost agree in the prediction of the wall pressure. Only a minor effect of the wall boundary condition can be noticed by the slight decrease in the wall pressure in the case of the cold wall.

Mach number and pressure distribution of the calculations with the SST model (reference calculations) are shown in Figs. 13 and 14 for adiabatic wall conditions, and in Figs. 15 and 16 for cold wall conditions. As in the clean flow case, no difference in the pressure distribution can be noticed, whereas the boundary-layer thickness, and, therefore, the friction losses, are increased in the cold wall case.

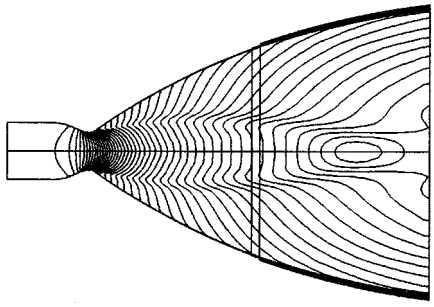

Fig. 13 Mach number distribution, adiabatic wall, film-cooled nozzle.

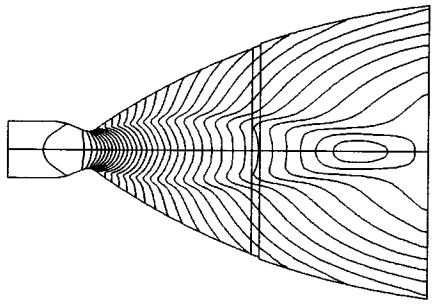

Fig. 14 Pressure distribution (log p/p_∞) adiabatic wall, film-cooled nozzle.

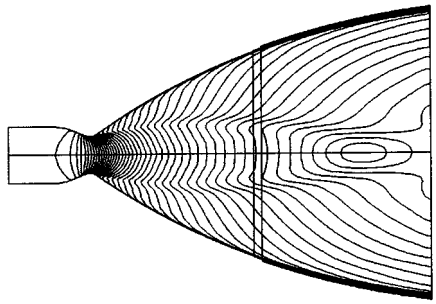

Fig. 15 Mach number distribution, cold wall, film-cooled nozzle.

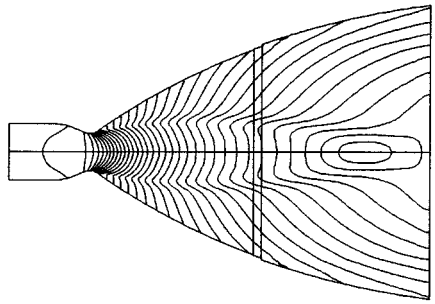

Fig. 16 Pressure distribution (log p/p_∞), cold wall, film-cooled nozzle.

V. Concluding Remarks

It has been shown that the nozzle performance prediction is influenced significantly by the choice of the turbulence model. The verification test case has demonstrated that the differences between algebraic and two-equation models are mainly caused by the overprediction of friction losses by algebraic models.

While discrepancies between algebraic and two-equations models are moderate for adiabatic flow, large deviations exist in the case of a cold wall condition. This indicates not only that turbulence modeling has an impact on the performance prediction itself, but also that the influence is strongly dependent on the wall condition.

Therefore, a design for both clean and film-cooled nozzles must be based on predictions using a two-equation turbulence model. Because the variation of the predictions between the two-equation models tested is very low, all of the two-equation models seem to be adequate for future investigations of nozzle flow.

References

[1]Haidinger, F. A., Hartmann, G., and Weiland, C., "PERNOD—A High Performance Nozzle Optimization Design Technique," DGLR-JT95-067, DGLR Jahrestagung 1995, Bonn, Bad Godesberg, Germany, Sept. 1995.

[2]Aupoix, B., Mignosi, A., Viala, S., Bouvier, F., and Gaillard, R., "Experimental and Numerical Study of Supersonic Film Cooling," AIAA Paper 96-0657, Jan. 1996.

[3]Hagemann, G., Krülle, G., and Hannemann, K., "Numerical Flowfield Analysis of the Next Generation Vulcan Nozzle," AIAA Paper 95-2782, July 1995.

[4]Yang, R.-J., "Assessment of Turbulence and Chemistry Models for Film-Cooled Nozzle Flows," *Journal of Thermophysics and Heat Transfer*, Vol. 10, No. 2, 1996, pp. 284–289.

[5]Yee, H. C., "Upwind and Symmetric Shock-Capturing Schemes," NASA TM-89464, May 1987.

[6]Davis, S. F., "TVD Finite Difference Schemes and Artificial Viscosity," ICASE Rept. 84-20, NASA Langley Research Center, Hampton, VA, June 1984.

[7]Roe, P. L., "Approximate Riemann Solvers, Parameter Vectors and Difference Schemes," *Journal of Computational Physics*, Vol. 43, No. 2, 1981, pp. 357–372.

[8]Liou, M. S., Van Leer, B., and Shuen, J. S., "Splitting of Inviscid Fluxes for Real Gases," *Journal of Computational Physics*, Vol. 87, No. 1, 1990, pp. 1–24.

[9]Gordon, S., and McBride, B. J., "Computer Program for Calculation of Complex Chemical Equilibrium Compositions, Rocket Performance, Incident and Reflected Shocks, and Chapman-Jouguet Detonations," NASA SP 273, 1971.

[10]Schröder, W., and Behr, R., "A Numerical Method to Compute Overexpanded Nozzle Flow," First Asian Computational Fluid Dynamics Conf., Hong Kong, Jan. 1995.

[11]Schröder, W., and Hartmann, G., "Implicit Solutions of Three-Dimensional Viscous Hypersonic Flows," *Computers and Fluids*, Vol. 21, No. 1, 1992, pp. 109–132.

[12]Baldwin, B. S., and Lomax, H., "Thin Layer Approximation and Algebraic Model for Separated Turbulent Flows," AIAA Paper 78-0257, Jan. 1978.

[13]Yakhot, V., and Orszag, S. A., "Renormalization Group Analysis of Turbulence. I. Basic Theory," *Journal of Scientific Computing*, Vol. 1, No. 3, 1986, pp. 3–51.

[14]Kirtley, K. R., "Renormalization Group Based Algebraic Turbulence Model for Three-Dimensional Turbomachinery Flows," *AIAA Journal*, Vol. 30, No. 6, 1992, pp. 1500–1506.

[15]Wilcox, D. C., "Reassessment of the Scale-Determining Equation for Advanced Turbulence Models," *AIAA Journal*, Vol. 26, No. 11, 1988, pp. 1299–1310.

[16]Wilcox, D. C., "Progress in Hypersonic Turbulence Modeling," AIAA Paper 91-1785, June 1991.

[17]Wilcox, D. C., "Comparison of Two-Equation Turbulence Models for Boundary Layers with Pressure Gradient," *AIAA Journal*, Vol. 31, No. 8, 1993, pp. 1414–1421.

[18]Menter, F. R., "Two-Equation Eddy-Viscosity Turbulence Models for Engineering Applications," *AIAA Journal*, Vol. 32, No. 8, 1994, pp. 1598–1605.

[19]Haidinger, F. A., "Numerische Untersuchung turbulenter Stoß/Grenzschicht-Wechselwirkungen," Ph.D. Dissertation, Technische Univ. München, Lehrstuhl für Fluidmechanik, Munich, Germany, 1993.

[20]Haidinger, F. A., and Friedrich, R., "Numerical Simulation of Strong Shock/Turbulent Boundary Layer Interactions Using a Reynolds Stress Model," *Zeitschrift für Flugwissenschaften und Weltraumfahrt*, Vol. 19, No. 1, 1995, pp. 10–18.

[21]Zeman, O., "Dilatation Dissipation: The Concept and Application in Modeling Compressible Mixing Layers," *Physics of Fluids A*, Vol. 2, No. 2, 1990, pp. 178–188.

[22]Sarkar, S., Erlebacher, G., Hussaini, M. Y., and Kreiss, H. O., "The Analysis and Modeling of Dilatational Terms in Compressible Turbulence," *Journal of Fluid Mechanics*, Vol. 227, 1991, pp. 473–493.